Asian Journal of Andrology (2019) 21, 309–318
www.asiaandro.com; www.ajandrology.com

*Open Access*

**ORIGINAL ARTICLE**

Sperm Biology

# PLZF$^{pos}$c-KIT$^{pos}$-delineated $A_1$–$A_4$-differentiating spermatogonia by subset and stage detection upon Bouin fixation

**Rui-Ling Tang, Li-Qing Fan**

**While hallmarks of rodent spermatogonia stem cell biomarkers' heterogeneity have recently been identified, their stage and subset distributions remain unclear. Furthermore, it is currently difficult to accurately identify subset-specific SSC marker distributions due to the poor nuclear morphological characteristics associated with fixation in 4% paraformaldehyde. In the present study, testicular cross-sections and whole-mount samples were Bouin fixed to optimize nuclear resolution and visualized by immunohistochemistry (IHC) and immunofluorescence (IF). The results identified an expression pattern of PLZF$^{high}$c-KIT$^{pos}$ in $A_1$ spermatogonia, while $A_2$–$A_4$-differentiating spermatogonia were PLZF$^{low}$c-KIT$^{pos}$. Additionally, this procedure was used to examine asymmetrically expressing GFRA1 and PLZF clones, asymmetric $A_{pr}$ and false clones were distinguished based on the presence or absence of TEX14, a molecular maker of intercellular bridges, despite having identical nuclear morphology and intercellular distances that were <25 μm. In conclusion, this optimized Bouin fixation procedure facilitates the accurate identification of spermatogonium subsets based on their molecular profiles and is capable of distinguishing asymmetric and false clones. Therefore, the findings presented herein will facilitate further morphological and functional analysis studies and provide further insight into spermatogonium subtypes.**
*Asian Journal of Andrology* (2019) **21**, 309–318; doi: 10.4103/aja.aja_103_18; published online: 29 January 2019

**Keywords:** asymmetric division; cellular homolog of feline sarcoma viral oncogene v-kit; false clones; glial cell line-derived neurotrophic factor receptor alpha 1; promyelocytic leukemia zinc finger; spermatogonia stem cell

## INTRODUCTION

Spermatogonial stem cells (SSCs),[1] which are testis-specific adult stem cells, are responsible for the balance between self-renewal and differentiation toward the production of haploid spermatozoa throughout the mammalian lifetime. Spermatogonia can be divided into four subsets as follows: SSCs ($A_s$ spermatogonia), undifferentiated spermatogonia ($A_s$, $A_{pr}$, and $A_{al4-16}$ spermatogonia), $A_1$–$A_4$-differentiating spermatogonia, and intermediate (In) and B spermatogonia.[2,3] Additionally, there are also four major events that occur during a seminiferous cycle, namely (1) SSC self-renew throughout the seminiferous cycle; (2) undifferentiated spermatogonia proliferate during Stages X–II; (3) $A_{al}$ cells arrest in $G_0/G_1$ phase from Stage III forward; and (4) $A_{al}$ cells transform into $A_1$-differentiating spermatogonia without division during Stages VII–VIII.[4,5] These events are followed by six tightly controlled mitotic divisions in Stages IX, XI, I, II, IV, and VI to form $A_2$, $A_3$, $A_4$, In, B spermatogonia, and preleptotene spermatocytes, respectively, that irreversibly enter meiosis.[6–8]

In mice, a great deal of effort has been devoted to establishing a SSC molecular profile, with a combination of genetic mouse models, fluorescence-activated cell sorting (FACS), magnetic-activated cell sorting (MACS), *in vitro* SSC cultures, and SSC transplantation assays. Based on these findings, a number of SSC biomarkers have been identified.[9] Candidate SSC molecular markers have been found to be expressed in the spermatogonia along the basement membrane of the seminiferous tubules, stage-specific distribution is examined by cellular associations in seminiferous cycle, and subset distribution is identified by their topographical arrangements possessing an internuclear distance <25 μm in whole-mount tissues obtained from intact seminiferous tubules.[9] The undifferentiated or differentiating state can then be further defined by the co-expression of well-established SSC markers, such as promyelocytic leukemia zinc finger (PLZF, an undifferentiated spermatogonial marker) and c-KIT (cellular homolog of feline sarcoma viral oncogene v-kit, a differentiating spermatogonial marker) via cross-section and whole-mount immunofluorescence (IF).[9–11]

PLZF is present in $A_s$, $A_{pr}$, and $A_{al4-16}$ undifferentiated spermatogonia,[9,11] while c-KIT is expressed in $A_1$–$A_4$-differentiating spermatogonia ($A_{diff}$), as well as in In and B spermatogonia and preleptotene spermatocytes (pL).[12,13] During neonatal development, these markers are co-expressed in a subset of spermatogonia.[14] Furthermore, in adult mice, c-KIT has been reported to be expressed in undifferentiated spermatogonia,[12] while PLZF expression has been seen in differentiating spermatogonia.[15–17] Moreover, it has been suggested that a subpopulation of differentiating spermatogonia co-express PLZF/c-KIT,[16,18] but the exact identity of this specific subpopulation remains unclear.

Institute of Reproduction and Stem Cell Engineering, School of Basic Medicine Science, Central South University, Changsha 410078, China.
Correspondence: Dr. LQ Fan (fanliqingszzx@sina.com)
Received: 22 January 2018; Accepted: 30 September 2018

Bouin solution, a compound fixative, is routinely utilized to assess spermatogonial subsets in histology due to the robust nuclear morphological preservation that is obtained. Recently, Bouin and some other comparable fixatives have been reported to successfully detect testicular antigens and are replacing paraformaldehyde (PFA) and formalin fixation when performing cross-sectional immunochemistry (IHC) or IF.[19–22] Bouin has also been used in whole-mount IHC without hematoxylin nuclear-counterstaining.[23] The aim of this study was to identify subtype-specific and stage-specific SSC molecular marker distributions by a combination of paraffin section IHC and corresponding hematoxylin-counterstaining whole-mount IHC and 4,6-diamidino-2-phenylindole (DAPI)-counterstaining whole-mount IF using Bouin fixation to maintain nuclear morphology. First, Bouin was used to determine the exact stage and subtype distribution of PLZF and c-KIT expression in $A_s$, $A_{pr}$, $A_{al}$, $A_1$–$A_4$, In, and B spermatogonia in Stages I, III, V, VII, X, and XII (avoiding the mitotic division phases in Stages II, IV, VI, IX, and XI) using cross-section and whole-mount IHC counterstained by hematoxylin; the co-expression of PLZF/c-KIT, detected using whole-mount IF counterstaining with DAPI, was used to identify the subtype specificity of spermatogonia. Next, the compatibility of optimized Bouin procedure with other SSC molecules was further investigated using glial cell line-derived neurotrophic factor receptor alpha 1 (GFRA1), another marker of undifferentiated spermatogonia. Finally, in clones asymmetrically expressing GFRA1 or PLZF via hematoxylin-counterstaining whole-mount IHC, intercellular bridges labeled with testis-expressed gene 14 (TEX14) were examined using DAPI-counterstaining whole-mount IF.

## MATERIALS AND METHODS

### *Animals*

Eight- to ten-week-old adult male C57BL/6 mice ($n = 9$) were obtained from the Shanghai Laboratory Animal Center (SLAC, Shanghai, China), and three equal groups were established as follows: Group 1 was used to screen multiple players of spermatogenic epithelial cells and identify seminiferous stages following hematoxylin staining of whole-mount samples; Group 2 was used to establish stage and subset expression profiles for PLZF, c-KIT, and GFRA1 with cross-sections and whole-mount prepared samples and examined via hematoxylin or DAPI counterstaining IHC/IF; and Group 3 was used to observe nuclear morphology in GFRA1 and PLZF asymmetrically expressing clones in whole-mount IHC and intercellular bridges in GFRA1/TEX14 and PLZF/TEX14 whole-mount IF samples. Experimental protocols were approved by the Animal Care and Usage Committee of Central South University, Changsha, China (protocol number: LLSC (LA) 2016-031), and all animal procedures were performed in accordance with the approved guidelines and regulations.

### *Paraffin-embedded IHC*

Adult male C57BL/6 mice were sacrificed by cervical dislocation, and testes were dissociated, cut transversely, and fixed in Bouin for 8 h at 4°C. The tissue was then dehydrated, embedded in paraffin, and cut into 5-μm sections following deparaffinization. Testis sections were treated with 100 mmol $l^{-1}$ glycine at room temperature for 15 min and then 3% $H_2O_2$ for 10 min. The sections were then blocked with normal goat or rabbit serum (SP KIT-B2 or SP KIT-B5; Maixin Biotech, Fuzhou, China) for 2 h at room temperature. Next, the sections were incubated with primary antibodies, including rabbit anti-PLZF (1:200 dilution; SC-22839, Santa Cruz Biotechnology, Santa Cruz, CA, USA), goat anti-c-KIT (1:50 dilution; AF332, R&D Systems, Minneapolis, MN, USA), and goat anti-GFRA1 (1:50 dilution; AF714, R&D Systems) for 3 days at 4°C. Immunolabeling was detected by using biotinylated-linked secondary antibodies (SP KIT-C8 or SP KIT-C10; Maixin Biotech) and streptavidin-conjugated horseradish peroxidase (SP KIT-D2, Maixin Biotech). Sections were visualized using 3, 3'-diaminobenzidene hydrochloride (DAB; ZLI-9018, ZSGB-BIO, Beijing, China) and counterstained using Harris hematoxylin (BA4097, BASO, Zhuhai, China). All IHC sections were examined under a Sunny RX50 microscope (Sunny Optical Tech, Ningbo, China).

### *Whole-mount IHC and histology*

The testes were decapsulated, and the seminiferous tubules were carefully separated with microdissection forceps under an Olympus SZX10 stereomicroscope (Olympus, Tokyo, Japan). Several intact seminiferous tubules were fixed in Bouin at 4°C for 2–4 h and then incubated in 100 mmol $l^{-1}$ glycine at room temperature for 30 min. The samples were then dehydrated and rehydrated in a series of graded methanol (25%, 50%, 75%, and 100%). The tubules were then blocked in 0.3% bovine serum albumin (BSA; Sigma-Aldrich, St. Louis, MO, USA) and 5% donkey serum (Jackson Immunoresearch Laboratories, Lancaster, PA, USA) in PBS containing 0.05% triton X-100 (Sigma-Aldrich) overnight at 4°C. Then, the seminiferous tubules were incubated with primary antibodies, including rabbit anti-PLZF (1:200 dilution; SC-22839, Santa Cruz), goat anti-PLZF (1:50 dilution; AF2944, R&D Systems), goat anti-GFRA1 (1:50 dilution; AF560, R&D Systems), rabbit anti-TEX14 (1:100 dilution; ab41733, Abcam, Cambridge, UK), and goat anti-c-KIT (1:50 dilution; AF332, R&D Systems) for 3 days at 4°C. After the incubation, samples were washed 5 times with PBS containing 0.05% triton X-100 for 30 min. For whole-mount IHC, the seminiferous tubules were incubated with 3% $H_2O_2$ for 30 min and then incubated with biotinylated-linked secondary antibody and streptavidin-conjugated horseradish peroxidase (Maixin Biotech). Samples were visualized using DAB (ZSGB-BIO), counterstained with Harris hematoxylin (BASO, Zhuhai, China), mounted with aqueous mounting media (CW0137, CWBIO, Beijing, China), and imaged with a Sunny RX50 microscope (Sunny). For whole-mount IF, the primary antibodies were detected using donkey anti-goat conjugated to Alexa Fluor 594 or donkey anti-rabbit conjugated to Alexa Fluor 488 secondary antibodies (A21203 or A21206; Thermo Fisher Scientific, Waltham, CA, USA) and counterstained with DAPI (62248, Thermo Fisher Scientific). Images were obtained with a Leica TCS SP8 confocal microscope (Leica, Wetzlar, Germany). For whole-mount hematoxylin counterstaining histology, several 2–4 cm long seminiferous tubules were fixed in Bouin for 2 h at room temperature, dehydrated and rehydrated in a series of graded methanol, immersed in Harris hematoxylin (BASO) for 2 min, and differentiated in 0.1% acid ethanol for 30 s. The samples were then washed in tap water for 5 min, mounted with aqueous mounting media (CWBIO), and imaged with a Sunny RX50 microscope.

## RESULTS

### *Comparison of PLZF expression in paraffin IHC, whole-mount IHC, and whole-mount IF samples fixed with 4% PFA and Bouin*

In paraffin-embedded cross-sections and whole-mount IHC/IF samples fixed with 4% PFA, the spermatogonia and spermatocyte showed severe nuclear chromatin shrinkage and had a poor morphological appearance when compared with Bouin fixation. However, the ability to distinguish round and elongated spermatids did not differ between the two fixative methods (**Supplementary Figure 1–3**).

***Identification of spermatogonial subtypes during Stages I, III, V, VII, X, and XII in whole-mounted hematoxylin-counterstaining seminiferous tubules***

Several spermatogonial subtypes, including $A_1$–$A_4$, In, and B spermatogonia, were identified in Stages I, III, V, VII, X, and XII by their nuclear characteristics (**Supplementary Figure 4**), and their mitotic divisions were observed in Stages I, II, IV, VI, IX, and XI (data not shown). Seminiferous stages were identified based on spermatogenic cell associations as previously described.[24] Intermediate spermatogonia were identified based on their characteristic ovoid nuclei with chromatin flakes entirely around the nuclear membrane. To confirm the corresponding spermatocyte and spermatid association in Stage III, nuclear morphological characteristics were scanned along the Z-axis using a light microscope. Since the stages of a seminiferous cycle are distributed in an orderly fashion along the tubules, the stages of adjacent segments were identified accordingly. B spermatogonia and mid-primary spermatocytes were observed in Stage V. In $A_1$–$A_4$-differentiating spermatogonia, slightly oval or round nuclei with little heterochromatin adhering to the nuclear envelope were observed. Multiple layers of stage-specific spermatogenic cellular associations were scanned to identify $A_2$ in Stage X, $A_3$ in Stage XII, and $A_4$ in Stage I (**Supplementary Figure 5**) due to their similar nuclear morphological characteristics and clone sizes. In stage VII, X, XII and I, $A_1$–$A_4$-differentiating spermatogonia were linearly distributed and separated by Sertoli cells, while in Stages III–V, the In and B spermatogonia were packed tightly.

***Stage- and subtype-specific expression profile for PLZF, c-KIT, and GFRA1 during Stages I, III, V, VII, X, and XII in cross-sections and the corresponding whole-mount IHC***

In cross-section IHC samples, strong PLZF and weak PLZF staining were located in two distinct subpopulations of A spermatogonia, though not in the In and B spermatogonia. In whole-mount IHC samples, PLZF staining was intense in $A_s$, $A_{pr}$, and $A_{al4–16}$ spermatogonia across the seminiferous cycle and in $A_1$ spermatogonia in Stage VII. Weak PLZF staining was seen in $A_2$–$A_4$ clusters during Stages IX–I, with no PLZF staining detected in In- and B-differentiated spermatogonia during Stages III–V. Nuclear details were identified using hematoxylin counterstaining, which provided clear, distinct identification of spermatogonial subtypes. PLZF staining was intense in $A_{al}$ clusters that were separated by crowed In and B clones in Stages III–V. PLZF staining was strong in $A_1$ spermatogonia in Stage VII and weak in $A_2$–$A_4$ spermatogonia in Stages IX–I, with cells linearly distributed and separated by Sertoli cells (**Figure 1**). When hematoxylin counterstaining was not performed, loosely arranged and tightly lined PLZF strong clones mingled with PLZF weak clusters were observed, while their morphological subtypes were indistinct (**Supplementary Figure 6**).

In cross-section IHC samples, c-KIT was expressed in A, In, and B spermatogonia and PL spermatocytes around the seminiferous tubules. In whole-mount IHC samples, c-KIT expression was seen in $A_1$–$A_4$-differentiating spermatogonia during Stages VII–I, In and B spermatogonia during Stages III–V, and PL spermatocytes in Stage VII. In both the cross-section and whole-mount samples, no c-KIT immunostaining was detected in undifferentiated A type spermatogonia (**Figure 2**). In whole-mount samples without hematoxylin counterstaining, c-KIT-positive clusters with progressively increased sizes were observed, and their subtypes were ambiguous because of the lack of nuclear morphological details (**Supplementary Figure 7**).

In cross-section IHC samples, GFRA1 was expressed in a few of the A spermatogonia surrounding the seminiferous tubules. In whole-mount IHC samples, GFRA1 immunostaining was predominantly detected on the cytomembranes of $A_s$, $A_{pr}$, and $A_{al4}$ undifferentiated spermatogonial clones with homogeneous hematoxylin-staining nuclei across the seminiferous cycle (Stages I–XII). No GFRA1 staining was detected in $A_1$–$A_4$-differentiating spermatogonia during Stages VII–I, in In- or spermatogonia during Stages III–V (**Figure 3**). When hematoxylin counterstaining was not performed, GFRA1-positive $A_s$, $A_{pr}$, $A_{al4}$ spermatogonia, occasionally $A_{al8}$ and $A_{al16}$ spermatogonia clones were discerned by counting the clonal cells; it was not certain whether intercellular bridges existed between them (**Supplementary Figure 8**).

***Co-expression profile of PLZF/c-KIT and GFRA1/PLZF during Stages I, III, V, VII, X, and XII using whole-mount IF***

To determine an accurate subtype-specific molecular expression profile, dual immunostaining with PLZF/c-KIT or GFRA1/PLZF was performed using whole-mount IF. When using DAPI staining for nuclear visualization instead of hematoxylin in whole-mount samples preserved by Bouin, spermatogonial subtype staining patterns were very similar. Briefly, $A_{un}$ and $A_1$ spermatogonial nuclei were ovoid with uniformly distributed chromatin in the nuclei, while $A_2$–$A_4$-differentiating spermatogonia contained heterochromatin that appeared mottled and were located around the rim of the nuclear envelope. The In spermatogonia displayed heterochromatin flakes lining the nuclear envelop with a central heterochromatin dot, while the B spermatogonia periodically exhibited round and compact heterochromatin along the nuclear envelope and at the center of the nucleus. In the PL spermatocytes, the nuclei became smaller, but the nuclear details remained similar to those of the B spermatogonia. The DAPI-stained nuclear characteristics of the $A_2$–$A_4$ spermatogonia were similar, but the characteristic germ cell associations in Stages X, XII, and I made them distinguishable.

PLZF and c-KIT were co-stained in strongly PLZF$^{POS}$ $A_1$ spermatogonia in Stage VII and weakly PLZF$^{POS}$ $A_2$–$A_4$-differentiating spermatogonia during Stages IX–I. In strongly PLZF$^{POS}$ $A_s$, $A_{pr}$, and $A_{al}$ spermatogonia, no c-KIT co-staining was noted (**Figure 4**). Therefore, the exact co-expression of PLZF and c-KIT in $A_1$–$A_4$-differentiating spermatogonia can be delineated.

In whole-mount IF samples, GFRA1 was co-located with strong PLZF staining in $A_s$, $A_{pr}$, and $A_{al4}$ undifferentiated spermatogonia throughout the seminiferous cycles. No GFRA1 co-staining was detected in $A_1$–$A_4$-differentiating spermatogonia in stage VII, X, XII, and I regardless of PLZF intensity, and no GFRA1 was detected in PLZF$^{NEG}$ In- and B-spermatogonia or in PL spermatocytes during Stages III–VII (**Figure 5**). GFRA1$^{POS}$ $A_{al8}$ was also co-located with strong PLZF staining (**Supplementary Figure 9**).

***Asymmetric $A_{pr}$ and false clones distinguished by the presence or absence of TEX14 between GFRA1 and PLZF asymmetrically expressed daughter cells***

Asymmetric expression of GFRA1 and PLZF in spermatogonial clusters was observed in whole-mount IHC samples, with adjacent daughter cells connected by cellular bridges. In whole-mount IF samples, asymmetrically divided clones and false clones were further identified by TEX14/GFRA1 and TEX14/PLZF co-staining (**Figure 6**). GFRA1 asymmetrically divided $A_{pr}$ clones were composed of one GFRA1$^{POS}$ member and one GFRA1$^{NEG}$ member, with cellular bridges labeled with TEX14 between them. GFRA1 asymmetrically stained false $A_{un}$

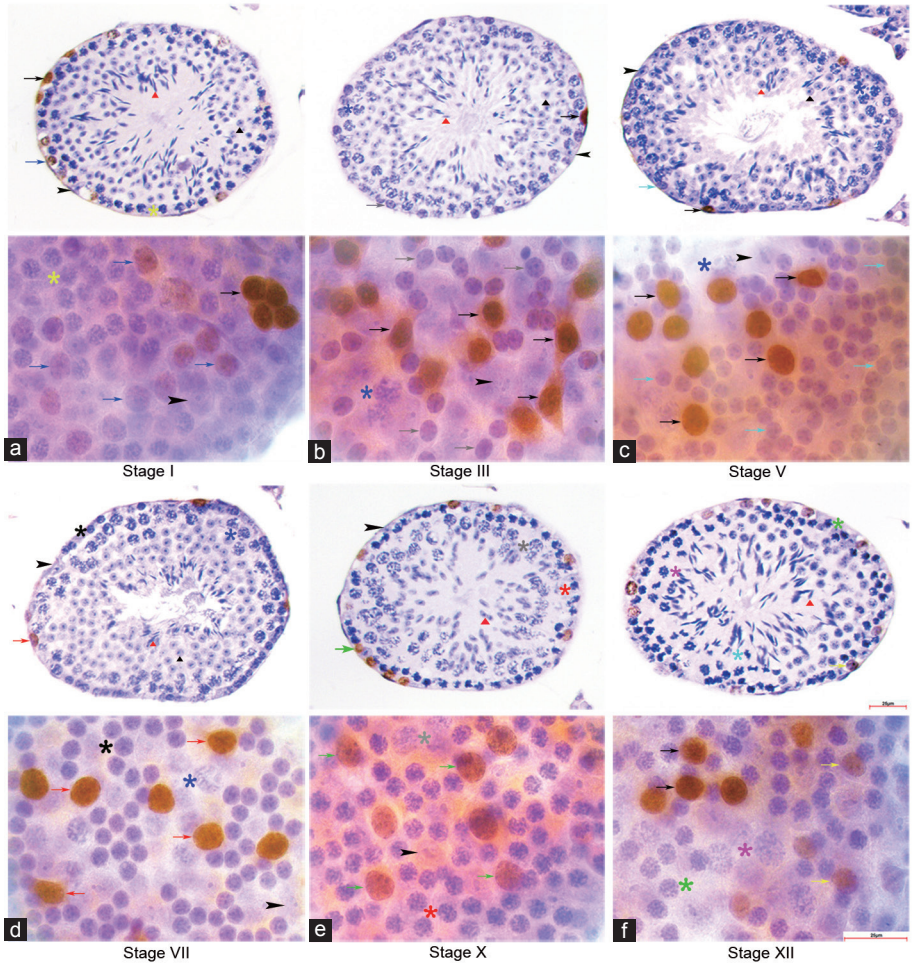


**Figure 1:** Expression profile of PLZF in cross section and whole mount IHC. PLZF was immune-stained strongly in undifferentiated A spermatogonia throughout the seminiferous cycle. (**a**) $A_4$ was PLZF$^{LOW}$ in stage I, (**b**) In was PLZF$^{NEG}$ in stage III, (**c**) B was PLZF$^{NEG}$ in stage V, (**d**) $A_1$ was PLZF$^{HIGH}$ in stage VII, (**e**) $A_2$ was PLZF$^{LOW}$ in stage X, (**f**) $A_3$ was PLZF$^{LOW}$ in stage XII in cross section and whole mount IHC. $A_{un}$: black arrows; $A_1$: red arrows; $A_2$: green arrows; $A_3$: yellow arrows; $A_4$: blue arrows; In: grey arrows; B: cyan arrows; preleptotene: black asterisks; leptotene: red asterisks; zygotene: green asterisks; early pachytene: yellow asterisks; mid-pachytene: blue asterisks; late pachytene: grey asterisks; diplotene: pink asterisks; meiotic division: cyan asterisks; Sertoli cells: black arrowheads; round spermatid: black triangles; elongating spermatid: red triangles. Scale bar=25 μm. PLZF: promyelocytic leukemia zinc finger; IHC: immunohistochemistry.

clones were comprised of GFRA1$^{POS}$ and GFRA1$^{NEG}$ $A_{un}$ clusters with similar homogeneous nuclear details. However, TEX14 staining was not detected between adjacent GFRA1$^{POS}$ and GFRA1$^{NEG}$ members despite an internuclear distance of <25 μm. In false PLZF clones, PLZF strongly stained $A_{un}$ clusters and weakly stained $A_{diff}$ clusters were arranged together, with TEX14-labeled intercellular bridges being absent between adjacent $A_{un}$ and $A_{diff}$ members with an internuclear distance of <25 μm. Furthermore, the nuclear details were different between the $A_{un}$ and $A_{diff}$ spermatogonia.

In whole-mount IHC samples, 5 $A_{pr}$ and 8 $A_{un}$ clones with asymmetric GFRA1 expression were identified out of a total of 196 GFRA1$^{POS}$ clones (5/196 = 2.55% and 8/196 = 4.08%, respectively), with intercellular bridges clearly observed. Out of 213 PLZF$^{POS}$ clones, 60 asymmetric $A_{un}$–$A_{diff}$ clones composed of strongly PLZF$^{POS}$ $A_{un}$ and weakly PLZF$^{POS}$ $A_{diff}$ clones (60/231 = 25.97%) were observed, with intercellular bridges being more ambiguous. In whole-mount IF samples, 3 asymmetrically divided $A_{pr}$ and 10 false $A_{un}$ clones were identified out of a total of 198 GFRA1$^{POS}$ clones (3/198 = 1.52% and 10/198 = 5.05%, respectively), with TEX14-labeled intercellular bridges present in $A_{pr}$ and lacking in $A_{un}$ between the GFRA1$^{POS}$ member and GFRA1$^{NEG}$ member. Of the 145 PLZF$^{POS}$ clones, 36 false clones lacking TEX14 staining between strongly PLZF stained $A_{un}$ and weakly stained $A_{diff}$ members with an internuclear distance of <25 μm were identified (36/145 = 24.83%; **Supplementary Figure 10**).

The distributions of GFRA1$^{POS}$ or PLZF$^{POS}$ clusters involved in the formation of asymmetric and false clones were evaluated using whole-mount IHC and IF samples (**Supplementary Figure 10**). In GFRA1-stained whole-mount IHC samples, 3.96% $A_s$ (4/101), 1.59% $A_{pr}$ (1/63), 3.33% $A_{al4}$ (1/30), and 16.67% $A_{al8}$ (2/12) spermatogonia were involved in $A_{un}$ clone with asymmetric GFRA1 expression. Out of a total of 196 GFRA1$^{POS}$ clones, 5 asymmetric $A_{pr}$ clones (5/196 = 2.55%) were listed separately which consisted of a GFRA1$^{POS}$ and a GFRA1$^{NEG}$ member. In PLZF-stained whole-mount IHC samples, 31.65% $A_s$ (25/79), 36.21% $A_{pr}$ (21/58), 13.95% $A_{al4}$ (6/43), 18.92% $A_{al8}$ (7/37), and 7.14% $A_{al>8}$ (1/14) spermatogonial clusters were involved in $A_{un}$–$A_{diff}$ clones with asymmetric PLZF expression. In GFRA1/TEX14 and PLZF/TEX14 whole-mount IF samples, asymmetric

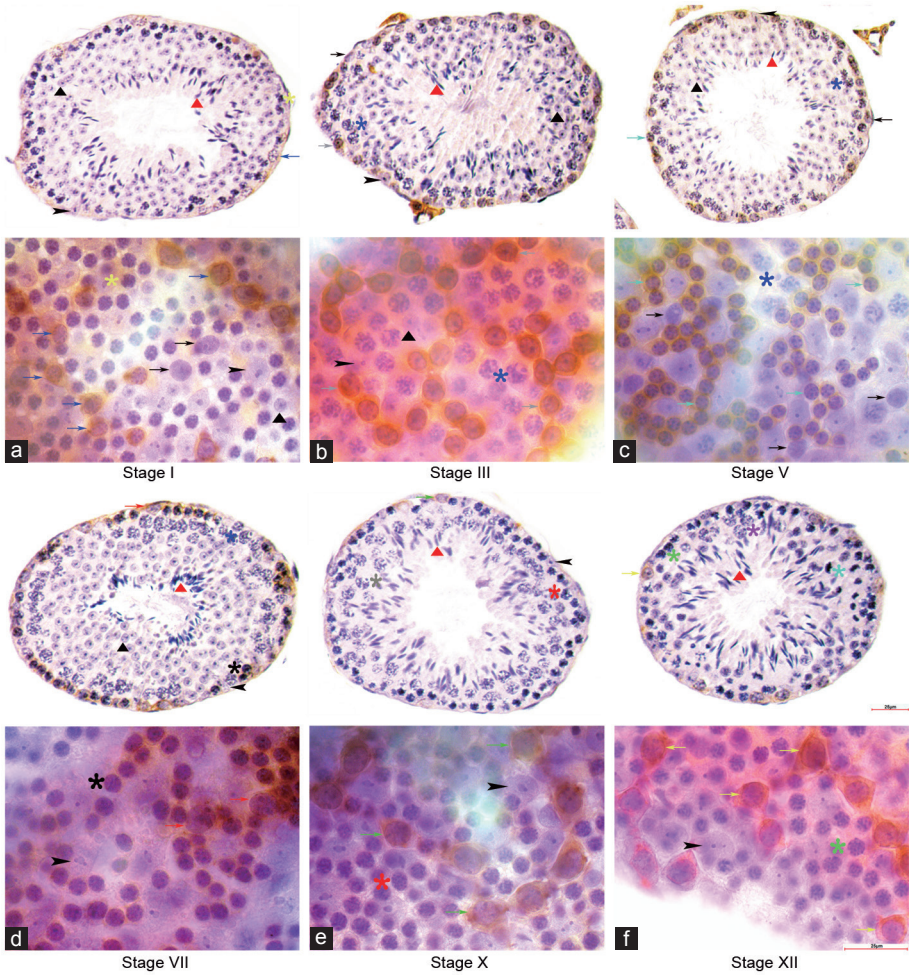


**Figure 2:** Expression profile of c-KIT in cross section and whole mount IHC. c-KIT immune-staining was detected on the cytomembrane of several subtypes of differentiating spermatogonia. c-KIT$^{POS}$ was observed in (**a**) $A_4$ in stage I, (**b**) In in stage III, (**c**) B in stage V, (**d**) $A_1$ and preleptotene in stage VII, (**e**) $A_2$ in stage X and (**f**) $A_3$ in stage XII in cross section and whole mount IHC. No c-KIT staining was detected in undifferentiated A spermatogonia across the seminiferous cycle. Indicators of multiple germ cell types were the same as in figure 1. Scale bar=25 μm.

GFRA1$^{POS}$ $A_{un}$ and PLZF$^{POS}$ $A_{un}$–$A_{diff}$ clones were demonstrated to be false clones, with TEX14 staining being absent between adjacent asymmetric members. Furthermore, GFRA$^{POS}$ $A_{un}$ false clones were formed by 3.70% $A_s$ (3/81), 1.64% $A_{pr}$ (1/61), 6.25% $A_{al4}$ (2/32), and 17.39% $A_{al8}$ (4/23) spermatogonia. Out of a total of 198 GFRA1$^{POS}$ clones, three were asymmetric $A_{pr}$ clones (3/198 = 1.52%) that were listed separately and consisted of a GFRA1$^{POS}$ member and a GFRA1$^{NEG}$ member connected by a TEX14-labeled intercellular bridge. In the formation of PLZF$^{POS}$ $A_{un}$–$A_{diff}$ false clones, 11.11% $A_s$ (5/45), 23.08% $A_{pr}$ (9/39), 30.77% $A_{al4}$ (8/26), 45% $A_{al8}$ (9/20), and 33.33% $A_{al>8}$ (5/15) were involved (**Supplementary Figure 10**).

When comparing whole-mount IF with whole-mount IHC, the percentage of GFRA1 asymmetric $A_{pr}$ clones was lower in IF relative to IHC (1.52% *vs* 2.55%), while the percentage of GFRA1 false $A_{un}$ clones was higher in IF (5.05% *vs* 4.08%). We supposed that asymmetric $A_{pr}$ in IHC was identified as false $A_{pr}$ in IF by the absence of TEX14 between them. Furthermore, when comparing whole-mount IF with whole-mount IHC, the percentage of PLZF$^{POS}$ $A_{al\geq8}$ clones associated with false clones increased, while the number of $A_s$ and $A_{pr}$ clones associated with false clones decreased. This may be due to the fact that some, members of $A_{al}$ clusters are far away from each other, therefore, some clonal members were mistaken for $A_s$ or $A_{pr}$ owing to indistinct intercellular bridges between them in IHC and were instead confirmed as larger $A_{al>8}$ clones due to the presence of intercellular TEX14 staining in whole-mount IF.

## DISCUSSION

Heterogeneity of expression profiles has been revealed in SSC biomarker research.[15–17,25–27] there are two issues that need to be addressed: (1) how to accurately identify stage- and subtype-specific distributions of SSC molecular markers and (2) how to elucidate the regulatory signal pathways that are involved in each spermatogonial subtype during specific seminiferous stages. In the current SSC molecular study, stage-specific distributions was identified by labeling acrosomal development simultaneously.[28] However, undifferentiated spermatogonia are inextricably commingled with differentiating spermatogonia during the entire seminiferous cycle, and the poor nuclear resolution associated with 4% PFA fixation, whether on cross-section or in whole mount, makes it difficult to distinguish them. Except for heterogeneity, numerous bimodal expression patterns have also been reported recently.[16–18] For example, while PZLF and c-KIT are classical spermatogonial biomarkers that have been verified by genetic animal models and functional transplantation assays[29–31] and are widely used to identify $A_{un}$ and $A_{diff}$ spermatogonial subtypes, their exact expression profiles remain controversial.[12,15–18] In addition to

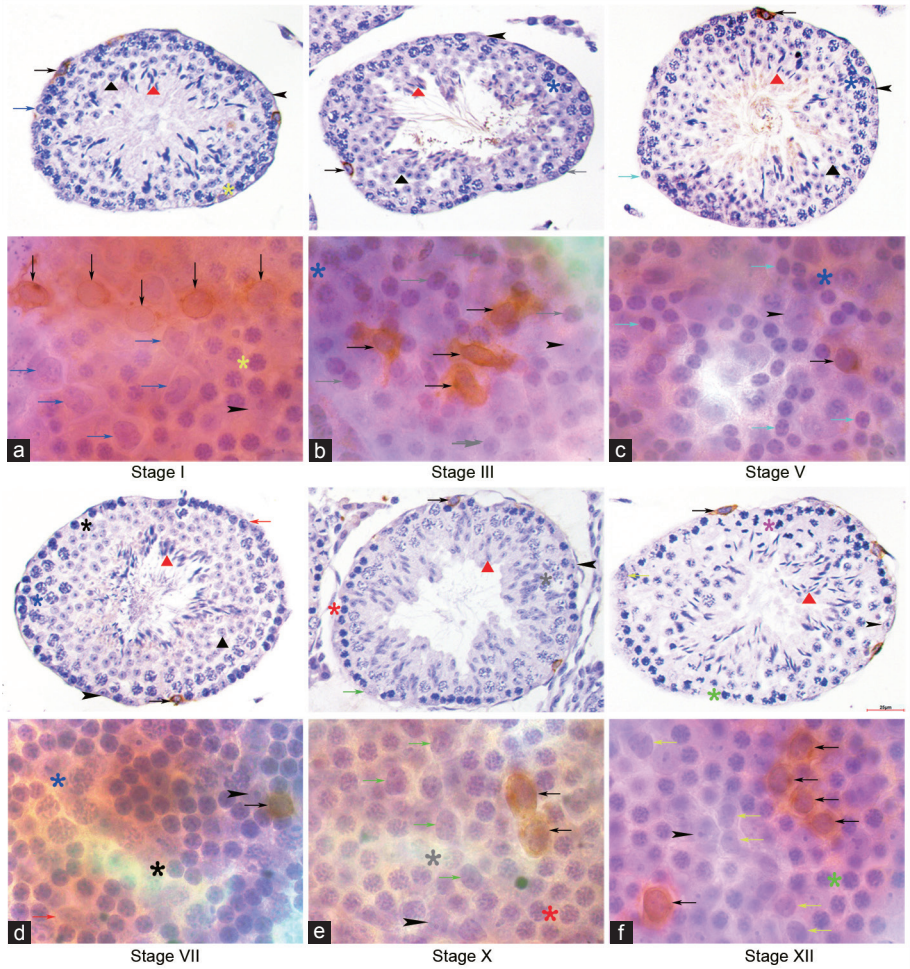


**Figure 3:** Expression profile of GFRA1 in cross section and whole mount IHC. GFRA1 immuno-staining was detected mostly on the cytomembrane of $A_s$, $A_{pr}$ and $A_{al4}$ undifferentiated spermatogonia clones across the seminiferous cycle. No GFRA1 staining was detected in (**a**) $A_4$ in stage I, (**b**) In in stage III, (**c**) B in stage V, (**d**) $A_1$ in stage VII, (**e**) $A_2$ in stage X and (**f**) $A_3$ in stage XII in cross section and whole mount IHC. Indicators of multiple germ cell types were the same as in figure 1. Scale bar=25 μm.

being expressed in undifferentiated spermatogonia, PLZF has also been found to be expressed in c-KIT-positive differentiating spermatogonia and three subgroups, including PLZF$^{pos}$c-KIT$^{neg}$, PLZF$^{pos}$c-KIT$^{pos}$, and PLZF$^{low}$c-KIT$^{pos}$, as identified by flow cytometry analysis.[18,32] However, the exact distributions among spermatogonial subpopulations and their corresponding functions remain unclear. Therefore, this study focused on establishing accurate expression profiles for PLZF and c-KIT in spermatogonial subpopulations.

In previous studies, the nuclear morphologies of spermatogonial subpopulations were identified using semi-thin plastic sections, with samples fixed in glutaraldehyde/$OsO_4$ and stained with toluidine,[33] or whole mount samples fixed in Bouin and stained with hematoxylin.[34] More recently, paraffin cross-sections or whole-mount samples were utilized and fixed with Bouin and visualized with IHC or IF.[12,35,36] In paraffin cross-section IHC samples, the nuclear morphology is compromised due to heat-induced antigen retrieval; in whole-mount IHC, hematoxylin counterstaining has not been performed to visualize the nuclear details. Thus, these methods alone make it difficult to identify molecular expression profile of spermatogonial subtypes accurately. In the present study, these measures were combined to solve this problem. First, chemical antigen retrieval was applied instead of heat retrieval to reduce the morphological damage induced by high temperature. Next, Bouin-fixed whole-mount IHC and IF were performed with hematoxylin and DAPI counterstaining. Our approach provided a nuclear morphology with SSC molecular immunostaining in paraffin section IHC, whole-mount IHC, and whole-mount IF samples fixed by Bouin, thus enabling the subtype- and stage-specific identification of immunopositive cells.

The use of Bouin fixation and chemical antigen retrieval in this study enabled the identification of spermatogonial subtypes within immunopositive cells by perfectly preserving their nuclear morphology. In Bouin-fixed seminiferous tubule cross-sections, A, In, and B spermatogonia and PL spermatocytes are roughly distinguishable based on their nuclear details, location, and association with multilayer germ cell types during a specific seminiferous stage. In whole-mount IHC samples, with the addition of hematoxylin counterstaining, $A_s$, $A_{pr}$, and $A_{al}$ undifferentiated spermatogonia and $A_1$–$A_4$-differentiating spermatogonia can be clearly detected based on their nuclear morphology and topographical clone arrangements. As $A_1$–$A_4$, In, and B spermatogonia collectively experience six successive division phases during Stages IX, XI, I, II, IV, and VI, respectively,[7] stage- and subtype-specific expression models were examined in Stages I, III, V, VII, X, and XII based on nonmitotic nuclear appearance. Additionally, since $A_2$–$A_4$ spermatogonial clone sizes increase slowly

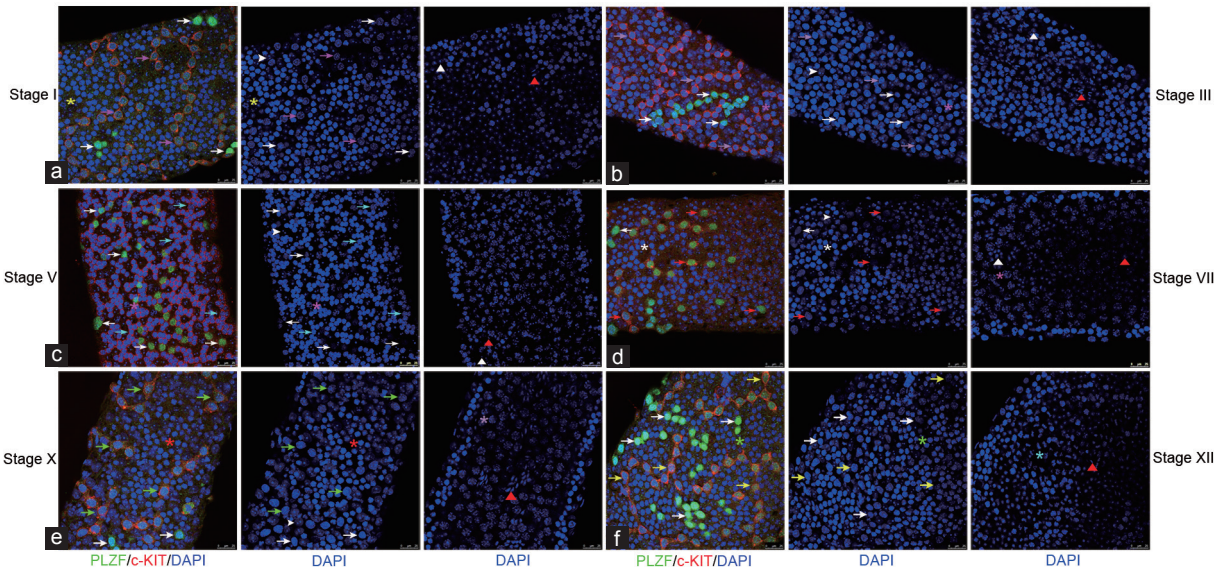


**Figure 4:** Co-expression profile of c-KIT/PLZF in whole mount IF. (**a**) A$_4$ was c-KIT$^{POS}$PLZF$^{LOW}$ in stage I, (**b**) In was c-KIT$^{POS}$PLZF$^{NEG}$ in stage III, (**c**) B was c-KIT$^{POS}$PLZF$^{NEG}$ in stage V, (**d**) A$_1$ was c-KIT$^{POS}$PLZF$^{HIGH}$ in stage VII, (**e**) A$_2$ was c-KIT$^{POS}$PLZF$^{LOW}$ in stage X, (**f**) A$_3$ was c-KIT$^{POS}$PLZF$^{LOW}$ in stage XII in cross section and whole mount IHC. no c-KIT was detected co-staining with PLZF$^{HIGH}$ undifferentiated A spermatogonia throughout the seminiferous cycle. A$_{un}$: white arrows; A$_1$: red arrows; A$_2$: green arrows; A$_3$: yellow arrows; A$_4$: pink arrows; In: grey arrows; B: cyan arrows; preleptotene: white asterisks; leptotene: red asterisks; zygotene: green asterisks; early pachytene: yellow asterisks; mid-pachytene: pink asterisks; late pachytene: grey asterisks; meiotic division: cyan asterisks; Sertoli cells- white arrowheads; round spermatid: white triangles; elongating spermatid: red triangles. Scale bar=25 μm.

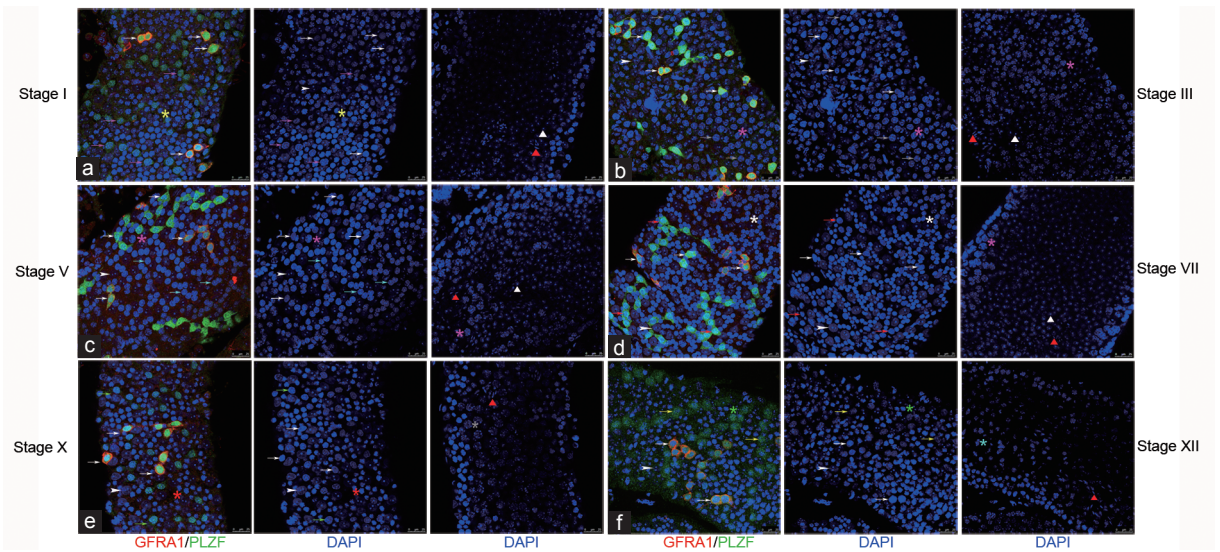


**Figure 5:** Co-expression profile of GFRA1/PLZF in whole mount IF. GFRA1 was co-located with strong PLZF expression in A$_s$, A$_{pr}$, and A$_{al4}$ undifferentiated spermatogonia throughout the seminiferous cycle. No GFRA1 was detected co-staining with (**a**) PLZF$^{HIGH}$ A$_4$ in stage I, (**b**) PLZF$^{NEG}$ In in stage III, (**c**) PLZF$^{NEG}$ B in stage V, (**d**) PLZF$^{LOW}$ A$_1$ in stage VII, (**e**) PLZF$^{LOW}$ A$_2$ in stage X and (**f**) PLZF$^{LOW}$ A$_3$ in stage XII in cross section and whole mount IHC. Indicators of multiple germ cell types were the same as in Co-expression profile of GFRA1/PLZF in whole mount IF. GFRA1 was co-located with strong PLZF expression in A$_s$, A$_{pr}$, and A$_{al4}$ undifferentiated spermatogonia throughout the seminiferous cycle. No GFRA1 was detected co-staining with (a) PLZF$^{HIGH}$ A4 in stage I, (b) PLZF$^{NEG}$ In in stage III, (c) PLZF$^{NEG}$ B in stage V, (d) PLZF$^{LOW}$ A$_1$ in stage VII, (e) PLZF$^{LOW}$ A$_2$ in stage X and (f) PLZF$^{LOW}$ A$_3$ in stage XII in cross section and whole mount IHC. Indicators of multiple germ cell types were the same as in figure 4. Scale bar = 25 um.

due to density-dependent apoptosis,[37] and A$_1$–A$_4$ spermatogonial nuclear morphology is comparable,[38,39] multiple layers of spermatogenic cellular nuclear morphology associations were scanned to identify A$_2$ clones in Stage X, A$_3$ clones in Stage XII, and A$_4$ clones in Stage I (**Supplementary Figure 5**).

When utilizing the above-mentioned optimized procedures, nuclear morphological characteristics can be clearly seen, thus enabling the accurate identification of mingled A$_{un}$ and A$_{diff}$ subtypes. This approach guarantees that stage- and subtype-specific SSC biomarker profile can be detected by the combination of paraffin-embedded testicular cross-sections and whole-mount IHC/IF. Furthermore, this study was able to accurately characterize the bimodal expression pattern of PLZF. PLZF expression was intense in A$_s$, A$_{pr}$, and A$_{al4–16}$ undifferentiated spermatogonia throughout the seminiferous cycle and in A$_1$ spermatogonia in Stage VII, while weak expression was seen in A$_2$–A$_4$-differentiating spermatogonia during Stages

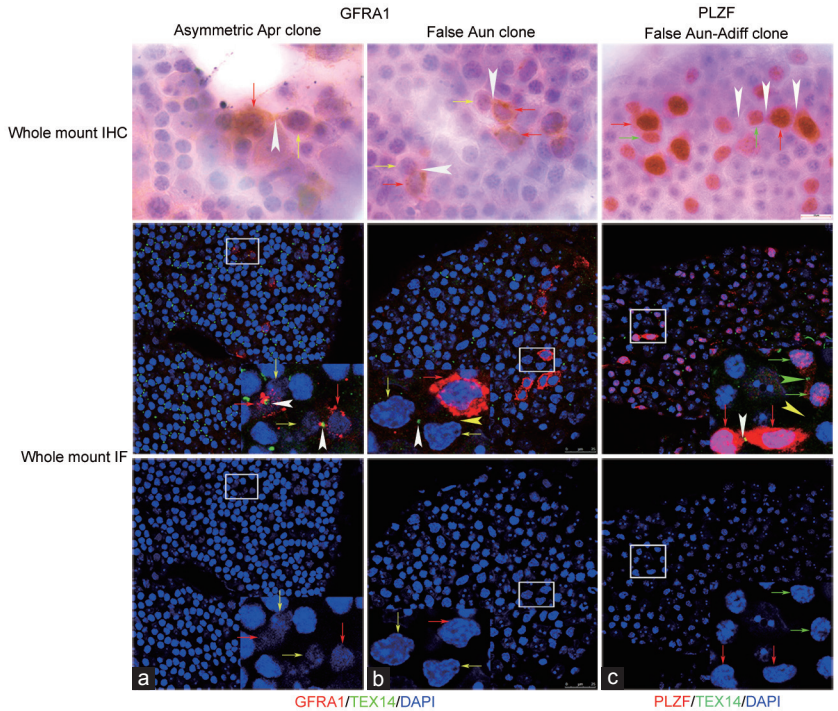


**Figure 6:** Asymmetrically divided $A_{pr}$ clones, false $A_{un}$ and $A_{un}$–$A_{diff}$ clones were identified by co-staining TEX14 with GFRA1 and PLZF. (**a**) GFRA1 asymmetrically positive $A_{pr}$ clones in whole-mount IHC were identified as asymmetrical division by the presence of TEX14. (**b**) GFRA1 asymmetrically stained $A_{un}$ clones in whole-mount IHC was identified as false $A_{un}$ clone by the absence of TEX14 between adjacent GFRA1$^{POS}$ and GFRA1$^{NEG}$ clonal members. (**c**) a PLZF asymmetrically expressed $A_{un}$–$A_{diff}$ clone in whole-mount IHC was identified as false $A_{un}$ and $A_{un}$–$A_{diff}$ clone by absence of TEX14 between adjacent $A_{un}$ and $A_{diff}$ clonal members. GFRA1$^{POS}$ or PLZF$^{HIGH}$ $A_{un}$: red arrows; GFRA1$^{NEG}$ $A_{un}$: yellow arrows; PLZF$^{LOW}$ $A_{diff}$ : green arrows; IB in whole mount IHC: white arrowheads; IB between $A_{un}$ connected by TEX14 in whole mount IF: white arrowheads; IB between $A_{diff}$ connected by TEX14 in whole mount IF: green arrowhead; IB between asymmetrical GFRA1 or PLZF cells without TEX14 in whole mount IF– yellow arrowhead. IB: intercellular bridge. Scale bar=25 μm.

IX–I. Additionally, c-KIT was found to be distributed in $A_1$–$A_4$-differentiating spermatogonia, as well as in In and B spermatogonia and PL spermatocytes across the whole seminiferous cycle, as previously reported.[13] When PLZF and c-KIT co-staining was performed, $A_s$–$A_{al16}$ undifferentiated spermatogonia were found to be PLZF$^{high}$c-KIT$^{neg}$, $A_1$-differentiating spermatogonia were PLZF$^{high}$c-KIT$^{pos}$, and $A_2$–$A_4$ differentiating spermatogonia were PLZF$^{low}$c-KIT$^{pos}$. Therefore, we delineated $A_1$-$A_4$ differentiating spermatogonia by PLZF$^{pos}$c-KIT$^{pos}$, In and B spermatogonia by PLZF$^{neg}$c-KIT$^{pos}$. Furthermore, GFRA1 expression and GFRA1/PLZF co-expression in $A_s$, $A_{pr}$, and $A_{al4-8}$ spermatogonia were consistent with that of previous findings.[10,27] Indeed, a bimodal staining model has also been found as an inhibitor of differentiation 4 (ID4) and Sal-like protein 4 (SALL4) expression profiles in mouse spermatogonia.[11,40] Bouin-fixed paraffin IHC sections were used to identify the expression of Stimulated by retinoic acid gene 8 (*STRA8*) and c-KIT in $A_1$–$A_4$ differentiating spermatogonial subpopulations. Nevertheless, the IHC signal was weak and nuclear detail was damaged by heat antigen retrieval.[12,41]

It has been reported that c-KIT$^{POS}$-differentiating spermatogonia can revert to functional stem cells and reconstruct spermatogenesis after transplantation into a germ cell-depleted mouse recipient, the repopulating activity increases when c-KIT is co-expressed with undifferentiated molecular markers, such as OCT-4, GFRA1, or α6-integrin.[31,42,43] Furthermore, density-dependent apoptosis is classically thought to exist when $A_1$–$A_4$-differentiated spermatogonia proliferate during Stages IX–I, with the number of $A_4$ spermatogonia being only about 3.4 times as many as the $A_1$ spermatogonia after three mitotic proliferations.[34] Moreover, In- and B-spermatogonia secrete chalone to inhibit the proliferation of neighboring $A_{al}$ undifferentiated spermatogonia, and $A_{al}$ clones are largely quiescent during Stages III–VI until they differentiate into $A_1$ spermatogonia at Stages VII–VIII.[44] In a knockout mouse model, Bax and Bcl-xL were reported to be involved in density-dependent apoptosis.[7] However, the molecular mechanisms and signaling pathways modulating the biological behaviors of these differentiating spermatogonial subpopulations remain unknown, and the specific chemical components of chalone have yet to be characterized. Therefore, it is able to identify and sort these spermatogonial subtypes using combined SSC markers of PLZF and cKIT to enable further characterization of their molecular mechanisms and biological behaviors.

In the "$A_s$ model," $A_s$ spermatogonia have been proposed to be true SSCs. In this model, the two daughter cells that are generated after division either migrate away and become two new $A_s$ stem cells or remain together and form $A_{pr}$ spermatogonia that are connected by an intercellular bridge with an internuclear distance <25 μm.[45,46] Furthermore, $A_{un}$ spermatogonial clusters have also been reported to asymmetrically express SSC markers.[10,27,47] Nevertheless, it remains unclear whether they are false clones with different nuclear details or absence of intercellular bridge, or true clones with similar nuclear characteristics and connected by an intercellular bridge. In this study, asymmetric GFRA1 expression in a few $A_{pr}$ spermatogonia was found to be accompanied by TEX14 staining between daughter cells; while asymmetrical GFRA1 expression in $A_{un}$ spermatogonial clones was composed by smaller $A_s$, $A_{pr}$, and $A_{al}$ clusters without TEX14 staining; thus, they were false clones. These findings further strengthen the asymmetric $A_{pr}$ division that is seen in the "$A_s$ model," but the

sample size herein was very small. These findings also support the "fragmentation model," which claimed that larger $A_{al}$ spermatogonial chains can fragment into $A_s$ and $A_{pr}$ spermatogonia and renew their SSC characteristics.[25,27,48] Thus, our future studies will focus on the *in vivo* dynamics of intercellular bridges within these spermatogonial clusters by using TEX14 and GFRA1 double transgenic mouse or other animal models.

## CONCLUSION

This study optimized the procedures that are utilized when studying SSC molecular expression by utilizing paraffin cross-sections and whole-mount IHC/IF samples that are Bouin fixed and counterstained by hematoxylin/DAPI. Furthermore, the exact co-expression pattern in $A_1$–$A_4$-differentiating spermatogonia was found to be PLZF$^{pos}$c-KIT$^{pos}$, and GFRA1 asymmetrical expression in $A_{pr}$ and $A_{al}$ was found to be associated with asymmetrical division and false clones, respectively. The subdivision of cytological markers verified herein will significantly contribute to further analysis of the four events that occur during the seminiferous cycle in continuous spermatogenesis, including SSC self-renewal, SSC progenitor proliferation, $A_{al}$ spermatogonial arrest in the $G_0/G_1$ phase, and $A_{al}$ spermatogonial differentiation to $A_1$.

## AUTHOR CONTRIBUTIONS

LQF designed and guided the research, and RLT performed the experiments. LQF and RLT analyzed the data and discussed the results. RLT wrote the paper, and LQF commented on the manuscript.

## COMPETING INTERESTS

The authors declare no competing interests.

## ACKNOWLEDGMENTS

This work was supported by the grants from the National Key Research and Development Program of China (Project No. 2016YFC1000200) and the National Natural Science Foundation of China (Project No. 31472054).

Supplementary Information is linked to the online version of the paper on the *Asian Journal of Andrology* website.

## REFERENCES

1 Van Eenennaam H, Vogelzangs JH, Bisschops L, Te Boome LC, Seelig HP, *et al.* Autoantibodies against small nucleolar ribonucleoprotein complexes and their clinical associations. *Clin Exp Immunol* 2002; 130: 532–40.
2 de Rooij DG. Stem cells in the testis. *Int J Exp Pathol* 1998; 79: 67–80.
3 Oakberg EF. A new concept of spermatogonial stem-cell renewal in the mouse and its relationship to genetic effects. *Mutat Res* 1971; 11: 1–7.
4 Lok D, de Rooij DG. Spermatogonial multiplication in the Chinese hamster. III. Labelling indices of undifferentiated spermatogonia throughout the cycle of the seminiferous epithelium. *Cell Tissue Kinet* 1983; 16: 31–40.
5 Tegelenbosch RA, de Rooij DG. A quantitative study of spermatogonial multiplication and stem cell renewal in the C3H/101 F1 hybrid mouse. *Mutat Res* 1993; 290: 193–200.
6 Lok D, de Rooij DG. Spermatogonial multiplication in the Chinese hamster. I. Cell cycle properties and synchronization of differentiating spermatogonia. *Cell Tissue Kinet* 1983; 16: 7–18.
7 de Rooij DG, Grootegoed JA. Spermatogonial stem cells. *Curr Opin Cell Biol* 1998; 10: 694–701.
8 Ahmed EA, de Rooij DG. Staging of mouse seminiferous tubule cross-sections. *Methods Mol Biol* 2009; 558: 263–77.
9 Phillips BT, Gassei K, Orwig KE. Spermatogonial stem cell regulation and spermatogenesis. *Philos Trans R Soc Lond B Biol Sci* 2010; 365: 1663–78.
10 Grisanti L, Falciatori I, Grasso M, Dovere L, Fera S, *et al.* Identification of spermatogonial stem cell subsets by morphological analysis and prospective isolation. *Stem Cells* 2009; 27: 3043–52.
11 Gassei K, Orwig KE. SALL4 expression in gonocytes and spermatogonial clones of postnatal mouse testes. *PLoS One* 2013; 8: e53976.
12 Schrans-Stassen BH, van de Kant HJ, de Rooij DG, van Pelt AM. Differential expression of c-kit in mouse undifferentiated and differentiating type A spermatogonia. *Endocrinology* 1999; 140: 5894–900.
13 Yoshinaga K, Nishikawa S, Ogawa M, Hayashi S, Kunisada T, *et al.* Role of c-kit in mouse spermatogenesis: identification of spermatogonia as a specific site of c-kit expression and function. *Development* 1991; 113: 689–99.
14 Niedenberger BA, Busada JT, Geyer CB. Marker expression reveals heterogeneity of spermatogonia in the neonatal mouse testis. *Reproduction* 2015; 149: 329–38.
15 Hermann BP, Mutoji KN, Velte EK, Ko D, Oatley JM, *et al.* Transcriptional and translational heterogeneity among neonatal mouse spermatogonia. *Biol Reprod* 2015; 92: 54.
16 Hobbs RM, La HM, Makela JA, Kobayashi T, Noda T, *et al.* Distinct germline progenitor subsets defined through Tsc2-mTORC1 signaling. *EMBO Rep* 2015; 16: 467–80.
17 Mutoji K, Singh A, Nguyen T, Gildersleeve H, Kaucher AV, *et al.* TSPAN8 expression distinguishes spermatogonial stem cells in the prepubertal mouse testis. *Biol Reprod* 2016; 95: 117.
18 Hobbs RM, Fagoonee S, Papa A, Webster K, Altruda F, *et al.* Functional antagonism between Sall4 and Plzf defines germline progenitors. *Cell Stem Cell* 2012; 10: 284–98.
19 Dutta D, Park I, Mills NC. Fixation temperature affects DNA integrity in the testis as measured by the TUNEL assay. *Toxicol Pathol* 2012; 40: 667–74.
20 Howroyd P, Hoyle-Thacker R, Lyght O, Williams D, Kleymenova E. Morphology of the fetal rat testis preserved in different fixatives. *Toxicol Pathol* 2005; 33: 300–4.
21 Latendresse JR, Warbrittion AR, Jonassen H, Creasy DM. Fixation of testes and eyes using a modified Davidson's fluid: comparison with Bouin's fluid and conventional Davidson's fluid. *Toxicol Pathol* 2002; 30: 524–33.
22 Mazaud-Guittot S, Gow A, Le Magueresse-Battistoni B. Phenotyping the claudin 11 deficiency in testis: from histology to immunohistochemistry. *Methods Mol Biol* 2011; 763: 223–36.
23 Hofmann MC, Braydich-Stolle L, Dym M. Isolation of male germ-line stem cells; influence of GDNF. *Dev Biol* 2005; 279: 114–24.
24 Clermont Y, Bustos-Obregon E. Re-examination of spermatogonial renewal in the rat by means of seminiferous tubules mounted "in toto". *Am J Anat* 1968; 122: 237–47.
25 Nakagawa T, Nabeshima Y, Yoshida S. Functional identification of the actual and potential stem cell compartments in mouse spermatogenesis. *Dev Cell* 2007; 12: 195–206.
26 Abid SN, Richardson TE, Powell HM, Jaichander P, Chaudhary J, *et al.* A-single spermatogonia heterogeneity and cell cycles synchronize with rat seminiferous epithelium stages VIII-IX. *Biol Reprod* 2014; 90: 32.
27 Nakagawa T, Sharma M, Nabeshima Y, Braun RE, Yoshida S. Functional hierarchy and reversibility within the murine spermatogenic stem cell compartment. *Science* 2010; 328: 62–7.
28 Mark M, Teletin M, Vernet N, Ghyselinck NB. Role of retinoic acid receptor (RAR) signaling in post-natal male germ cell differentiation. *Biochim Biophys Acta* 2015; 1849: 84–93.
29 Buaas FW, Kirsh AL, Sharma M, McLean DJ, Morris JL, *et al.* Plzf is required in adult male germ cells for stem cell self-renewal. *Nat Genet* 2004; 36: 647–52.
30 Costoya JA, Hobbs RM, Barna M, Cattoretti G, Manova K, *et al.* Essential role of Plzf in maintenance of spermatogonial stem cells. *Nat Genet* 2004; 36: 653–9.
31 Ohbo K, Yoshida S, Ohmura M, Ohneda O, Ogawa T, *et al.* Identification and characterization of stem cells in prepubertal spermatogenesis in mice. *Dev Biol* 2003; 258: 209–25.
32 Carnevalli LS, Trumpp A. Tuning mTORC1 activity for balanced self-renewal and differentiation. *Dev Cell* 2010; 19: 187–8.
33 Chiarini-Garcia H, Russell LD. High-resolution light microscopic characterization of mouse spermatogonia. *Biol Reprod* 2001; 65: 1170–8.
34 Huckins C, Oakberg EF. Morphological and quantitative analysis of spermatogonia in mouse testes using whole mounted seminiferous tubules, I. The normal testes. *Anat Rec* 1978; 192: 519–28.
35 Dettin L, Ravindranath N, Hofmann MC, Dym M. Morphological characterization of the spermatogonial subtypes in the neonatal mouse testis. *Biol Reprod* 2003; 69: 1565–71.
36 Muciaccia B, Boitani C, Berloco BP, Nudo F, Spadetta G, *et al.* Novel stage classification of human spermatogenesis based on acrosome development. *Biol Reprod* 2013; 89: 60.
37 De Rooij DG, Lok D. Regulation of the density of spermatogonia in the seminiferous epithelium of the Chinese hamster: II. Differentiating spermatogonia. *Anat Rec* 1987; 217: 131–6.
38 de Rooij DG. Spermatogonial stem cell renewal in the mouse. I. Normal situation. *Cell Tissue Kinet* 1973; 6: 281–7.
39 de Rooij DG, Russell LD. All you wanted to know about spermatogonia but were afraid to ask. *J Androl* 2000; 21: 776–98.
40 Helsel AR, Yang QE, Oatley MJ, Lord T, Sablitzky F, *et al.* ID4 levels dictate the stem cell state in mouse spermatogonia. *Development* 2017; 144: 624–34.
41 Endo T, Romer KA, Anderson EL, Baltus AE, de Rooij DG, *et al.* Periodic retinoic acid-STRA8 signaling intersects with periodic germ-cell competencies to regulate

spermatogenesis. *Proc Natl Acad Sci U S A* 2015; 112: E2347–56.
42 Morimoto H, Kanatsu-Shinohara M, Takashima S, Chuma S, Nakatsuji N, *et al*. Phenotypic plasticity of mouse spermatogonial stem cells. *PLoS One* 2009; 4: e7909.
43 Barroca V, Lassalle B, Coureuil M, Louis JP, Le Page F, *et al*. Mouse differentiating spermatogonia can generate germinal stem cells *in vivo*. *Nat Cell Biol* 2009; 11: 190–6.
44 de Rooij DG. Effect of testicular extracts on proliferation of spermatogonia in the mouse. *Virchows Arch B Cell Pathol Incl Mol Pathol* 1980; 33: 67–75.
45 De Rooij DG. Morphometric description of spermatogonial stem cells and expansion of their clonal derivatives. In: Orwig KE, Hermann BP, editors. Male Germline Stem Cells: Developmental and Regenerative Potential. Totowa, NJ: Humana Press; 2011. p. 89–105.
46 van Beek ME, Davids JA, de Rooij DG. Variation in the sensitivity of the mouse spermatogonial stem cell population to fission neutron irradiation during the cycle of the seminiferous epithelium. *Radiat Res* 1986; 108: 282–95.
47 Suzuki H, Sada A, Yoshida S, Saga Y. The heterogeneity of spermatogonia is revealed by their topology and expression of marker proteins including the germ cell-specific proteins Nanos2 and Nanos3. *Dev Biol* 2009; 336: 222–31.
48 Hara K, Nakagawa T, Enomoto H, Suzuki M, Yamamoto M, *et al*. Mouse spermatogenic stem cells continually interconvert between equipotent singly isolated and syncytial states. *Cell Stem Cell* 2014; 14: 658–72.

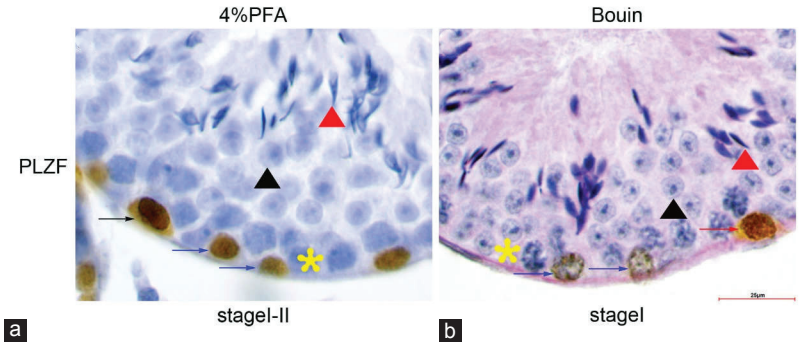


**Supplementary Figure 1:** Comparison of PLZF expression in paraffin sections fixed by 4% PFA and Bouin. (**a**) In cross sections fixed by 4% PFA, severe shrinkage of nuclear chromatin presented poor morphological appearance of the nuclei of spermatogonia and spermatogonocytes, $A_{un}$ and $A_{diff}$ were identified by their strong and weak immunostaining, respectively, early pachytene spermatocytes were discerned by their adhering to the basement membrane, and Stages I and II were speculated by the combination of round and elongated spermatids. (**b**) In cross section fixed by Bouin, nuclear chromatin details were perfectly preserved, $A_{un}$ with homogeneous chromatin, $A_4$ with a small amount of heterochromatin adhering to the nuclear membrane, early primary spermatocytes adjacent to basement membrane with unobvious sexual bodies, and Stage I was identified by the combination of round and elongated spermatids. $A_{un}$: black arrows; A4 spermatogonia: blue arrows; early pachytene spermatocytes: yellow asterisks; Sertoli cells: black arrowheads; round spermatids: black triangles; elongating spermatids: red triangles. Scale bar = 25 μm. PLZF: promyelocytic leukemia zinc finger; PFA: paraformaldehyde.

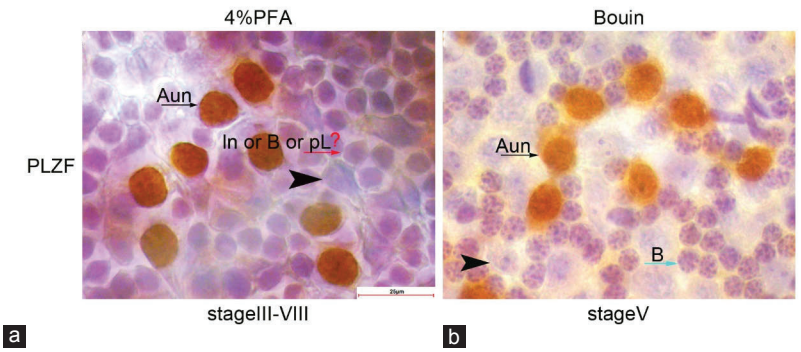


**Supplementary Figure 2:** Comparison of PLZF expression in whole-mount IHC fixed by 4% PFA and Bouin. (**a**) In whole-mount IHC samples fixed by 4% PFA, severe shrinkage of nuclear chromatin presented poor morphological appearance of the nuclei of spermatogonia, $A_{un}$ was identified by strong immunostaining and $A_{diff}$ was difficult to distinguish by nuclear staining details, spermatocytes were not detected along the basement membrane, and Stages III–VIII were postulated. (**b**) In whole-mount IHC samples fixed by Bouin, nuclear chromatin details were perfectly preserved, $A_{un}$ with homogeneous chromatin and B with multiple chromatin masses adhering to the nuclear membrane, and Stage V was identified. $A_{un}$: black arrows; differentiating spermatogonia: red arrows; B spermatogonia: cyan arrows; Sertoli cells: black arrowheads. Scale bar = 25 μm. PLZF: promyelocytic leukemia zinc finger; IHC: immunohistochemistry.

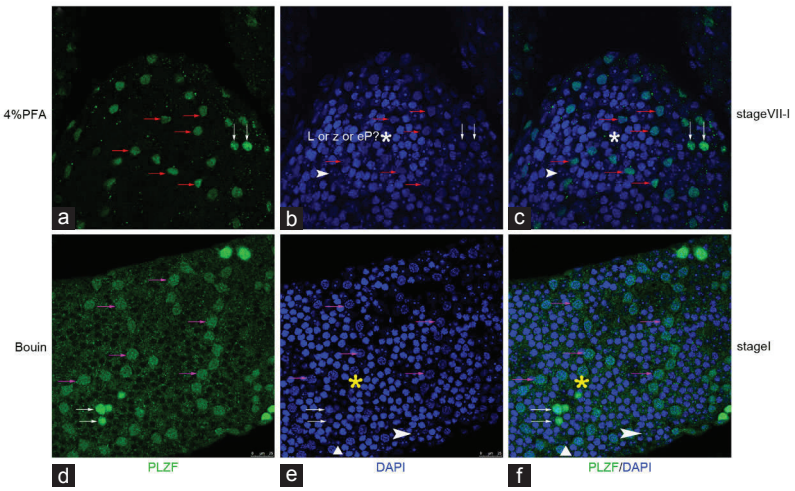


**Supplementary Figure 3:** Comparison of PLZF expression in whole-mount IF fixed by 4% PFA and Bouin. (**a**) In whole-mount IF samples fixed by 4% PFA, extensive shrinkages of seminiferous tubules and nuclear chromatin of various cell types were observed. $A_{un}$ and $A_{diff}$ with poor nucleus morphology were identified by their strong and weak immunostaining, respectively; it was difficult to distinguish the preleptotene or leptotene or zygotene or early pachytene spermatocytes by nuclear staining details, and stage VII, X, XII, or I, were speculated. (**b**) In whole-mount IF samples fixed by Bouin, nuclear chromatin details were perfectly preserved, $A_{un}$ with homogeneous chromatin, $A_4$ with a small amount of heterochromatin adhering to the nuclear membrane, early primary spermatocytes adjacent to basement membrane with unobvious sexual bodies, and Stage I was identified by the combination of round spermatids. Aun-black arrows; Adiff-red arrows; A4 spermatogonia: pink arrows; undistinguished preleptotene or leptotene or zygotene or early pachytene spermatocytes: white asterisks; early pachytene spermatocytes: yellow asterisks; Sertoli cells: white arrowheads; round spermatids: white triangles. Scale bar = 25 μm. PLZF: promyelocytic leukemia zinc finger; PFA: paraformaldehyde; IF: immunofluorescence.

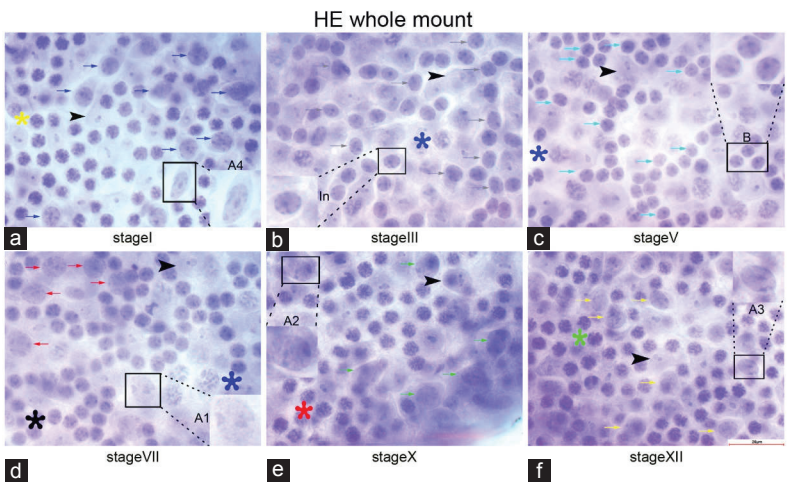


**Supplementary Figure 4:** Identification of Stages I, III, V, VII, X, and XII according to the nuclear morphological of (**a**) $A_4$differentiating spermatogonia in Stage I, (**b**) In spermatogonia in Stage III, (**c**) B spermatogonia in Stage V, (**d**) $A_1$-differentiating spermatogonia and preleptotene spermatocytes in Stage VII, (**e**) $A_2$-differentiating spermatogonia in Stage X, (**f**) $A_3$-differentiating spermatogonia in Stage XII in several 2–4 cm-long whole-mount seminiferous tubules stained by Harris hematoxylin from adult normal mouse. $A_1$–$A_4$-differentiating spermatogonia were linearly arranged, while In and B spermatogonia were tightly crowded. $A_1$–$A_4$-differentiating spermatogonia showed slightly oval or round nuclei, $A_1$ contained homogeneous chromatin throughout the nuclei without heterochromatin stick to envelop, $A_2$–$A_4$ with slightly heterochromatin clump adhering to the nuclear envelope; In differentiated spermatogonia contained heterochromatin lining entirely the nuclei; B differentiated spermatogonia showed round heterochromatin patches intermittently along the nuclear membrane. Insets showed higher magnifications of $A_4$ in Stage I, In in Stage III, B in Stage V, $A_1$ in Stage VII, $A_2$ in Stage X, and $A_3$ in Stage XII. A1: red arrows; A2: green arrows; A3: yellow arrows; A4: blue arrows; In: gray arrows; B: cyan arrows; preleptotene: black asterisks; leptotene: red asterisks; zygotene: green asterisks; early pachytene: yellow asterisks; mid-pachytene: blue asterisks; Sertoli cells: black arrowheads.Scale bar = 25μm.

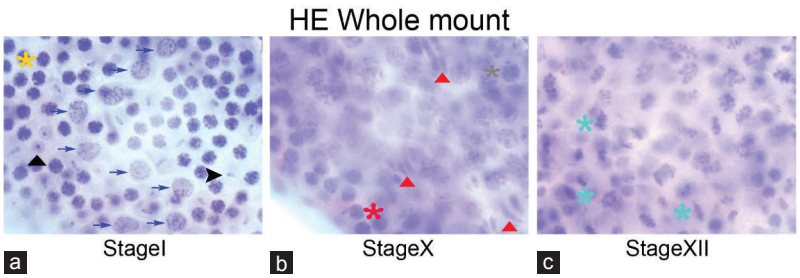


**Supplementary Figure 5:** Multiple layers of spermatogenic cells were scanned to better characterize Stages I, X, and XII. (**a**) Stage I was identified by the association of $A_4$ differentiating spermatogonia, early pachytene spermatocytes, and round spermatids; (**b**) Stage X was discerned by the association of leptotene spermatocytes, late pachytene spermatocytes, and step 10 spermatids with characteristic bilateral flattening spermatid heads because of condensing and elongating nuclei; (**c**) Stage XII was distinguished by unique meiotic division figures. $A_4$: blue arrows; leptotene: red asterisks; early pachytene: yellow asterisks; late pachytene: gray asterisks; elongating spermatids: red triangles; meiotic division figures: cyan asterisks; Sertoli cells: black arrowheads. Scale bar = 25um..

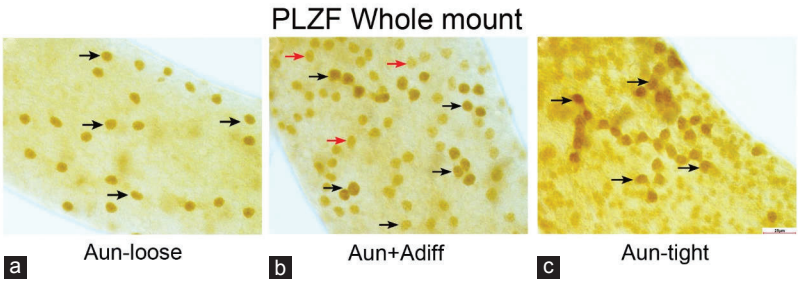


**Supplementary Figure 6:** In whole-mount IHC samples without hematoxylin counterstaining, (**a**) loosely arranged $PLZF^{HIGH}$ $A_{un}$, (**b**) $PLZF^{HIGH}$ clusters mingled with $PLZF^{LOW}$ clusters, (**c**) tightly arranged $PLZF^{HIGH}$ $A_{un}$ were arranged along the seminiferous tubules, while their morphological subtypes were indistinct. $PLZF^{HIGH}$: black arrows; $PLZF^{LOW}$: red arrows. Scale bar = 25 μm. PLZF: promyelocytic leukemia zinc finger.

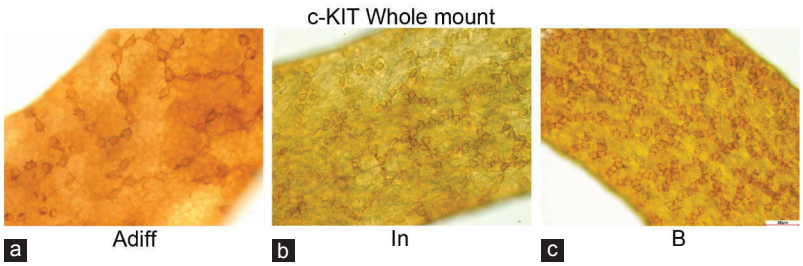


**Supplementary Figure 7:** In whole-mount IHC samples without hematoxylin counterstaining, c-KIT-positive subtypes were identified by clone sizes because of the lack of nuclear morphological details, (**a**) $A_{diff}$ (**b**) In, and (**c**) B spermatogonia were speculated by counting $c\text{-}KIT^{POS}$ clonal cells. Scale bar = 25 μm. IHC: immunohistochemistry.

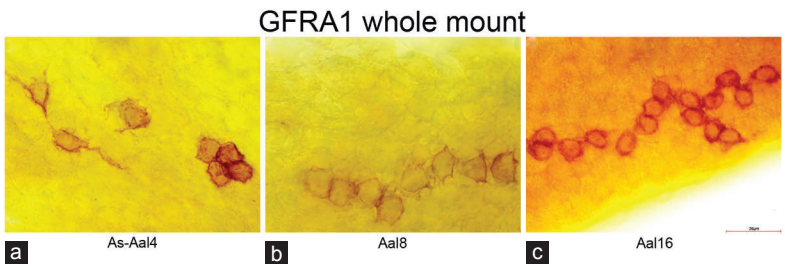


**Supplementary Figure 8:** In whole-mount IHC samples without hematoxylin counterstaining, GFRA1-positive subtypes, including (**a**) As, Apr, and Aal4 spermatogonia, occasionally (**b**) Aal8 and (**c**) Aal16 clusters, were discerned by counting GFRA1-positive clonal cells. Scale bar = 25 μm. IHC: immunohistochemistry.

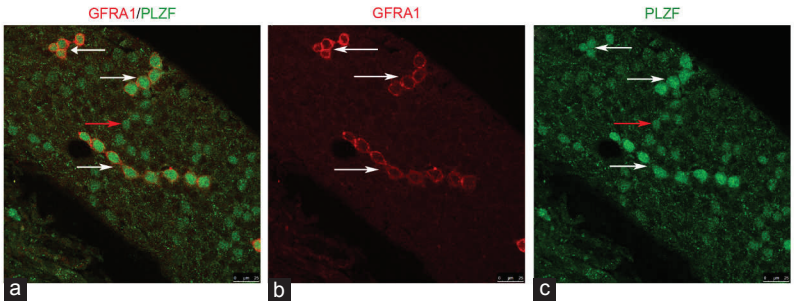


**Supplementary Figure 9:** In whole-mount IF samples without DAPI counterstaining, Aal4 and Aal8 clusters were speculated by counting GFRA1$^{POS}$PLZF$^{HIGH}$ clonal cells. Fluorescent channels labeled by (**a**) GFRA1 and PLZF, (**b**) GFRA1, (**c**) PLZF were showed respectively. Scale bar = 25 um.

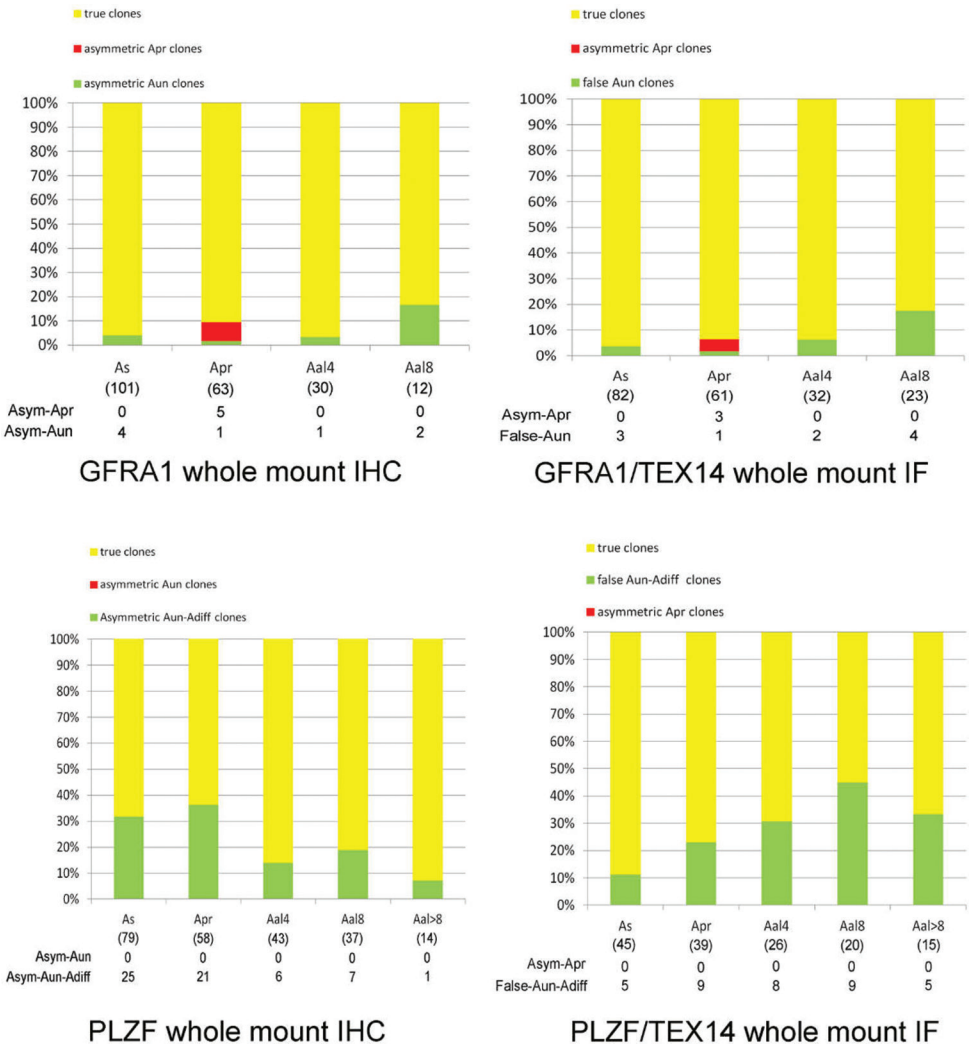


**Supplementary Figure 10:** Quantitative evaluation of asymmetric $A_{pr}$ clones and false clones using GFRA1, PLZF, and TEX14 staining in whole-mount IHC and IF. The number of GFRA1$^{POS}$ and PLZF$^{HIGH}$ clusters in asymmetric $A_{pr}$, $A_{un}$ and $A_{un}$-$A_{diff}$ clones in whole mount IHC, and asymmetric $A_{pr}$, false $A_{un}$ and false $A_{un}$–$A_{diff}$ clones in whole mount IF were evaluated and listed under the horizontal axis. Data were obtained from three adult male mice. Asym–Apr: asymmetrically expressed GFRA1 or PLZF in $A_{pr}$ spermatogonia observed via whole-mount IHC and connected by TEX14 staining via whole-mount IF; Asym–Aun: asymmetrically expressed GFRA1 or PLZF in $A_{un}$ spermatogonia observed via whole-mount IHC; Asym Aun-Adiff: clones with asymmetrical PLZF expression composed of strongly positive $A_{un}$ members and weakly stained $A_{diff}$ members observed via whole-mount IHC; false $A_{un}$–$A_{diff}$: asymmetrically expressed PLZF in $A_{un}$–$A_{diff}$ clones without positive TEX14 staining between strongly positive $A_{un}$ members and neighboring weakly stained $A_{diff}$ members observed via whole-mount IF. Aun–Adiff: PLZF$^{POS}$ clones composed by PLZF$^{HIGH}$ clusters mingling with PLZF$^{LOW}$ clusters. PLZF: promyelocytic leukemia zinc finger; IHC: immunohistochemistry; IF: immunofluorescence.